Journal of Engineering Research and Reports

20(4): 70-84, 2021; Article no.JERR.65675
ISSN: 2582-2926

Application of Machine Learning (ML) for Enhancing the Transient Performance of Thermal Energy Storage (TES) Platforms Using Radial Basis Function (RBF)

N. Shettigar[1], M. Truong[1], A. Thyagarajan[1], A. Bamido[1] and Debjyoti Banerjee[1-7*]

[1]J. Mike Walker '66 Department of Mechanical Engineering (MEEN), U.S.A.
[2]Harold Vance Department of Petroleum Engineering (PETE), U.S.A.
[3]Engineering-Medicine Program (ENMED), College of Engineering (COE), U.S.A.
[4]Department of Medical Education (DME), College of Medicine (COM), U.S.A.
[5]Mary Kay O'Connor Process Safety Center (MKOPSC), U.S.A.
[6]Gas and Fuels Research Center (GSFC), U.S.A.
[7]Energy Institute (EI); Texas A&M University, College Station, TX 77843-3123, U.S.A.

Authors' contributions

This work was carried out in collaboration among all authors. Author NS designed the study, performed the statistical analysis, wrote the protocol and wrote the first draft of the manuscript. Authors MT, AT, AB and NS collaborated for performing the experiments. Author DB managed the conception, formulation, execution and analyses of the study. Author NS managed the literature searches. All authors read and approved the final manuscript.

Article Information

DOI: 10.9734/JERR/2021/v20i417296
Editor(s):
(1) Dr. Hamdy Mohy El-Din Afefy, Pharos University, Egypt.
Reviewers:
(1) Ashrafoalsadat Shekarbaghani, Education Studies Research Center, Organization for Educational Research and Planning (OERP), Iran.
(2) M. Gajendiran, Sri Venkateswara College of Engineering, India.
Complete Peer review History: http://www.sdiarticle4.com/review-history/65675

Original Research Article

Received 16 December 2020
Accepted 22 February 2021
Published 23 March 2021

ABSTRACT

Thermal energy storage (TES) can be utilized as supplemental platforms for improving operational reliability and systemic efficiency in variety of industries, such as for reducing water usage in power production (food-energy-water/ FEW nexus), chemical and agro-process industries and for improving sustainability (e.g., desalination), etc. Phase change materials (PCMs) can be used in

**Corresponding author: Email: dbanerjee@tamu.edu;*

TES due to their high latent heat storage capacity during phase transformation. Inorganic PCMs typically have the highest latent heat capacity and are attractive for their ability to store the larger quantities of thermal energy in small form factors while conferring respectable power ratings (however, they suffer from compromised reliability issues, that often arise from the need for subcooling). Subcooling (also known as supercooling) is a phenomenon where the temperature needs to be reduced substantially below the melting point to initiate solidification. A technique for obviating subcooling issues is to allow a small portion of the PCM to remain un-melted. This allows the PCM to initiate nucleation from the un-melted portion of PCM (this is termed as the "cold finger" technique). Thus, reliability is enhanced at the expense of substantial reduction in storage capacity. A fundamental challenge for using this technique is the inability to reliably predict and control the amount of melt fraction in the total volume of the PCM (such that a target amount of the PCM remains solidified or un-melted at the end of each melt-cycle during repeated melting and solidification of the total mass of PCM). However, using Machine Learning (ML) techniques, this deficiency can be addressed by reliably predicting and thus controlling the amount of melt fraction in the total volume of the PCM with a higher accuracy than conventional techniques (such as using multi-physics-based models or numerical solvers). Conventional techniques for predicting transient characteristics in real time control schemes typically leverage multi-physics-based models that are often effective only for a narrow range of operating conditions with concomitant disadvantages: they are highly sensitive to small variations in the measurement uncertainties and are therefore susceptible to large levels of error in the real time predictions (and are unreliable for implementation in diverse range of operating conditions). In this pioneering study, nearest neighbor search processes (such as radial basis functions) were utilized along with machine learning (ML) algorithm using a training data set to predict the PCM melt fraction and to demonstrate the feasibility (and efficacy) of this approach. This technique is simple to implement and is device independent as well as robust (i.e., it can be deployed successfully even under conditions where the sensors malfunction, such as thermocouples that are off-calibration). This technique was demonstrated successfully for predicting the melt fraction of a PCM with high accuracy and robustness. With this method, the melt fraction of a PCM can be accurately determined, which allows the maximum thermal capacity of a PCM to be utilized while mitigating reliability issues (such as subcooling) and enhancing the thermodynamic efficiencies of the TES platforms. Melting experiments were performed using a digital camera (for video recording) and a graduated cylinder containing PCM for monitoring the transient values of the melt fraction based on the height of the liquid phase of the PCM in the cylinder. An array of 3 thermocouples was mounted at specific heights within the body of the PCM to monitor the temperature transients at these specific location during the propagation of the melt front within the PCM. In the final stages of the melting process, the predictions from the ML algorithm was found to be more accurate (90~95% accuracy) than that of the conventional techniques based on physics-based solvers (~60% accuracy). The accuracy of the ML algorithm was low at smaller melt fractions (~30%) and improved substantially at higher melt fractions (~95%). Furthermore, the accomplishments of this study display the feasibility of a RBF ML method which can be implemented for the accurate prediction and control of a real world stochastic system which can exhibit nonlinear and chaotic dynamics which change over time.

Keywords: Machine learning; radial basis function; thermal energy storage; phase change materials; experimental validation, stochastic prediction.

ABBREVIATIONS

PCM : Phase Change Material
TES : Thermal Energy Storage
ML : Machine Learning
ANN : Artificial Neural Network
Θ : Root mean square sum of temperature differences at any instant
Ψ : Root mean square sum of temperature differences at any instant between training data and test case
DAQ : Data Acquisition
NI : National Instruments

1. INTRODUCTION

Phase Change Materials (PCM) are typically used in Thermal Energy Storage (TES) platforms since they confer the advantage of storing significant amounts of thermal energy in small form factors. PCM selection is often guided by the large enthalpy and the temperature for phase change (in addition to cost and reliability considerations). An ideal PCM for TES applications should possess high latent heat capacity. Associated considerations include: high specific heat capacity, high thermal conductivity, and small changes in specific volume during phase transition. Also, an ideal PCM has minimal environmental footprint (e.g., should be non-toxic and noncorrosive) [1].

Careful consideration is needed for the choice of PCM for a specific TES platform or application. Each type of PCM has its own unique advantages and disadvantages. PCMs are often classified as organic, inorganic and eutectics. Organic PCMs (such as paraffins) are considered to be reliable but suffer from poor thermal characteristics (low storage capacity and poor power ratings). Inorganic PCMs (such as salt hydrates) typically possess very high latent heat capacity and higher thermal conductivity (than organic PCMs); however, suffer from reliability issues (due to subcooling issues and phase segregation [2] which occurs as a result of incongruent melting). This compromises the energy storage capacity of the TES during the phase change process (i.e., for initiating the nucleation within the volume of PCM during solidification cycle). Also, some salt hydrates can experience chemical degradation when repeatedly heated or cooled for multiple cycles of solidification and complete melting [3]. Salt hydrates also have poor nucleation characteristics. Significant volumetric changes during phase change and their corrosivity (especially to metal heat exchangers) are major impediments for universal applicability of salt hydrates in TES platforms as their long-term performance and reliability are often uncertain [4]. Prior attempts for controlling the subcooling of salt hydrates by the addition of suitable nucleating agents have shown some promise but are often associated with a cost burden of processing additional materials [5,6,7]. Also, the problem of phase segregation still remains unresolved. Various encapsulation techniques have been proposed and developed but the reliability and additional costs associated with these techniques can be a significant impediment [8].

The low thermal conductivity of paraffin waxes results in lower power ratings for TES platforms [3]. Several authors have studied if the efficacy (and power ratings) of heat exchangers impregnated with PCM can be enhanced by using different types of configurations, such as, using finned tubes [9], metal matrices or metal foams and carbon foams [10]. In addition, petroleum-derived paraffin can have a significant environmental footprint, since their processing is associated with water usage and release of a significant amount of carbon to the atmosphere, both of which also potentially contribute to global warming issues [4].

During the solidification process, some PCMs (especially inorganic PCMs) typically require some amount of subcooling (also known as supercooling) in order to initiate the nucleation process. After complete melting and as the solidification process is initiated, the PCM remains in the liquid phase when initially cooled to its phase transition temperature and a solidification is initiated only after the PCM is subcooled significantly below the phase transition temperature. This requires some amount of time (due to the thermal inertia of the mass of PCM) and hence, a significant portion of the time required for the solidification process is wasted in the process of initiating the phase transition (thus compromising the overall power rating of the TES platform as well as the operational reliability of the system). Subcooling is thus undesirable for practical engineering applications. The degree of subcooling is defined as the difference in the phase transition temperature and the temperature at which nucleation occurs (which can vary from one cycle to next during thermocycling, i.e., during repeated solidification and complete melting of the volume of PCM contained in a system, such as in a heat exchanger). The level of subcooling is typically ascertained using the T-History method [11] where the transient temperature profile of the PCM is recorded in a temperature-controlled environment (such as in an oven). Subcooling is affected by various considerations, such as: homogeneous nucleation, heterogeneous nucleation, surface finish (of the container), presence of impurities (which can initiate nucleation and suppress subcooling) and the experimental conditions (e.g., temperature ramp rates). Impact of surface finish on the degree of subcooling was reported by Faucheux et al. [12] in their study involving freezing of aqueous ethanol. Influence of cooling rate on the thermo physical properties were reported by

Taylor et al. [13]. The effect of other experimental conditions such as mass, time of experiments, superheat temperature, etc. were reported by García-Romero et al. [14].

It is necessary to implement methods to induce nucleation and control the crystallization process in salt hydrates due to the impact of subcooling on the thermal performance of Latent Heat Thermal Energy Storage Systems (LHTESS). Subcooling in salt hydrates are addressed by adopting seeding techniques and leveraging dynamic nucleation methods. Seeding is the process of reducing the subcooling of the PCM by adding nucleating agents. Seeding is promoted more reliably by nucleating agents that possess similar lattice structure as the solidified PCM, in order to effectively reduce the degree of subcooling. This limits the choice of additives for a given PCM to attain suitable reduction in the degree of subcooling Mehling and Cabeza [15] Lane [16] performed a detailed review of seeding techniques. Other reports include: Shamberger and O'Malley [17] on Lithium Nitrate Trihydrate, Shin et al. [18] on Glauber Salt, Schroder and Gawron [19], Kimura and Kai [20] and Lane [21] on Calcium Chloride Hexahydrate.

An attractive strategy for reducing subcooling in salt hydrates is the "cold finger technique". In this dynamic nucleation technique, a chosen mass fraction of the PCM is maintained in solid state at the end of the melt cycle, and this solid mass of PCM is utilized for seamlessly initiating the nucleation process during the freezing cycle Meseguer, et al. [22]. However, this technique is limited in use as this is feasible only when the phase transition temperature of the PCM is above the ambient temperature. Other reports in the literature include dynamic nucleation techniques, such as, using high pressure and shock waves to initiate the solidification of PCM Günther, et al. [23]. Fig. 1 shows the typical temperature profile (transient) profile during the melting process for PCMs [24]. However, this plot would suffer from hysteresis issues in the event subcooling occurs during the solidification process.

As mentioned before, an attractive technique for obviating subcooling issues is to allow a small portion of the PCM to remain un-melted, which then allows the PCM to solidify and nucleate starting from the un-melted portion of PCM (this is termed as the "cold finger" technique). Thus, the reliability of the TES platform is improved at a marginal expense to the storage capacity (since, complete melting of the total mass of PCM would have yielded higher storage capacity). One way to maximize the energy storage capacity of the TES would be to maximize the melt fraction without completely melting the PCM. This necessitates a reliable method for predicting the melt fraction as a function of time (as well as the time required to reach a particular melt fraction) in real time and based on the past history of the TES platform, such that a target amount of the PCM remains solidified or un-melted at the end of the duty cycle. Multi-physics-based models are finicky as they are very sensitive to measurement uncertainties and are often unreliable for deployment in real time predictions and commercial operations. These types of techniques that typically use multi-physics-based prediction strategies are often effective for a narrow range of operating conditions with concomitant disadvantages: they are highly sensitive to small variations in measurement uncertainties, are finicky and are often unreliable for a variety of real-world operating conditions. However, using Machine Learning (ML) techniques, these issues can be obviated by reliably predicting [25] and thus controlling with higher accuracy than conventional techniques.

In this study, nearest neighbor search processes (such as radial basis functions) were implemented in a Machine Learning (ML) based training algorithm. This technique is device independent and capable of predicting the melt fraction of a PCM with high accuracy and robustness. With this method, the melt fraction of a PCM can be determined accurately, which can be used for maximizing the energy storage capacity of a PCM in TES, while also mitigating reliability issues such as subcooling. Using this technique, the prediction of melt fraction for a PCM can be achieved with sufficiently high accuracy. The objective is to enable an user to predict the time required to reach a target melt fraction at any instant (based on the temperature distribution within a mass of PCM at that instant based on the history of the temperature transients within the PCM in prior melt cycles. This enables the energy storage capacity of the TES to be maximized (with certain degree of factor-of-safety) while minimizing the impediments to the reliable operation in each duty cycle (i.e., by targeting that a very small portion of the PCM remain un-melted in each cycle during melting in multiple duty cycles; where the environmental conditions can change by a wide margin – thus being robust in response

to wide variations in heat loss from the system depending on changes in the environmental conditions). This innovative and pioneering approach will allow for the maximization of the high storage capacity of PCMs (especially inorganic PCMs) while also improving their operational reliability (i.e., by obviating the drawbacks of subcooling issues which prevent their long-term applicability). The experimental results presented in this study demonstrate the robustness, feasibility and the high accuracy of the predictions for the range of melt fractions that have been implemented in this study. This enables the elimination of subcooling (and therefore improving the operational reliability) and in turn, maximizing the thermal performance (e.g., thermal energy storage capacity) of the PCM. Furthermore, this innovation is device independent and does not require the use of a complex new infrastructure to implement and integrate into a control system. In addition, this method is not affected by sensor malfunction (e.g., loss of calibration) of the temperature sensors (as long as, the temperature sensor reproduces the temperature trends with reasonable fidelity). Existing control systems can be retrofitted with this innovative technique and can be seamlessly integrated in real time (for real-time control) while the TES platform or system is in operation.

2. EXPERIMENTAL PROCEDURE AND METHODOLOGY

2.1 Experimental Apparatus and Procedure

For the implementation of the machine learning algorithm (i.e., for reliably predicting the transient values of the melt fraction of a PCM undergoing melting), an initial test apparatus was constructed. PCM was placed in a measuring beaker (with a volume of 50 ml and a least count of 0.5 ml). This enabled the determination of the melt fraction of the PCM by visual observation of the meniscus of the liquid PCM (this is aided by the significant volumetric expansion upon melting). Four K-type thermocouples were utilized in these experiments. Three K-type thermocouples were mounted at specific locations within the beaker corresponding to 30%, 60% and 85% melt fractions. The fourth K-type thermocouple was used for recording the ambient air temperature. A plastic jig was 3D printed and was used to mount the thermocouples at specific locations. A nichrome spool was placed in the bottom of the beaker and was connected to an external power supply (which served as a heat source for melting the PCM). The PCM used was PureTemp29 with a melting point of 29℃. After the experimental apparatus was constructed (Fig. 3) and assembled, several experiments were conducted by varying experimental conditions during the melt cycles. The data obtained from these experiments were used for training the ML algorithm. The temperature distribution of the PCM and the melt fraction of the PCM was observed and recorded in these experiments.

2.2 Data Analysis and Numerical Procedure

Data analysis was performed using the experimental results to identify the key trends in the transient values of the melt fraction and the transient temperature distribution within the volume of the PCM (contained in a graduated cylinder). A new variable was proposed, and termed as the "$[\Delta T]^2$ variable" or "θ"(Fig. 2). This variable is the sum of the square of the differences for each of the data points (at a given instant in time) for each of the three thermocouple recordings within the PCM. This variable is used to predict the transient values of the phase transformation at a given location within the volume of the PCM. When a particular location within the PCM is undergoing phase transformation, the value of θ (i.e., the value of θ $[\Delta T]^2$) at that particular location and at that instant in time is significantly greater than 1. As the PCM approaches the final stages of melting (or in the initial stages of melting), the values of θ (i.e., the value of θ $[\Delta T]^2$) are observed to approach 1. As the whole mass of PCM achieves complete melting, the value of θ (i.e., the value of θ $[\Delta T]^2$) is observed to be less than 1. This additional parameter θ therefore aids in reliable identification of the melt fraction of the PCM, thus improving the robustness of the ML algorithm. After the data acquisition in the experiments, a small portion of the data was allocated exclusively as the training data set. This exclusively allocated data was used as input for training the neural network algorithm (i.e., using a nearest neighbor radial basis function classification method). Equation (1) provides a formal mathematical description of this parameter, θ, (and is plotted in Fig. 2), as shown next:

$$\theta = \Sigma\ [\Delta T]^2 = (T_0 - T_1)^2 + (T_1 - T_2)^2 + (T_2 - T_0)^2 \qquad (1)$$

where, T_0, T_1, and T_2 are the transient values of temperatures recorded by the thermocouples

mounted at locations corresponding to 30%, 60% and 85% melt fractions, respectively.

For the successful implementation of the ML algorithm, the training data set along with training labels were generated initially. This was performed using the thermocouple data recorded by the digital data acquisition (DAQ) apparatus. The DAQ apparatus was procured from National Instruments (NI DAQ Board). The data recorded by the DAQ was automated using LabVIEW control software. Following this step, the temperature distributions within the PCM were recorded with respect to time using the thermocouple array that was mounted at precise locations within the PCM (i.e., in the measuring cylinder) using a 3D printed fixture. As an example, Fig. 4 shows the transient plot of the three thermocouples mounted at different heights within the body of the PCM. The height of the liquid meniscus of the PCM within the measuring cylinder (with graduated markings) was visually observed and recorded using a digital image acquisition apparatus to obtain the transient profile of the melt fraction. The melt fraction was calculated based on the liquid level in the measuring cylinder (as the PCM undergoes significant volumetric change during the melting process). A typical transient plot of melt fraction is shown in Fig. 5.

Hence, this enabled the generation of the training data set with corresponding training labels. Correlating the transient temperature data with the transient melt fraction data (Figs. 4 and 5), enabled the predictions with desirable accuracy. The temperature distribution recorded by the three thermocouples as well as the values of θ were plotted as a function of the melt fraction in Figs. 3 and 4. The training data consists of the temperature values (at each location of the thermocouple array mounted within the PCM volume) and the values of the θ (i.e., θ $[\Delta T]^2$) parameter of the PCM, and the training labels are the respective values of the melt fraction of the PCM for each temperature data point (in essence, the data set inherently obviated the time stamps during the training step). Feeding this into the neural network, correlations were generated between a given temperature distribution and the respective value of the melt fraction of the PCM.

3. RESULTS AND DISCUSSION

The data processing for the initial training data sets for the neural network is then cross referenced and checked for validity and accuracy using another set of data recorded from separate experiments (validation data set). For the test case, only the transient temperature distribution of the PCM is provided and the algorithm is used to predict the melt fraction based on the correlations obtained from the training set. The predicted values are then checked with the actual values of melt fraction of the PCM (in order to determine the accuracy and validity of the predictions). The nearest neighbor radial basis function technique was used in this study and is shown below in Equations 2 and 3 (T denotes training data, while T' denotes test data that is used for obtaining predictions for the instantaneous values of the melt fraction). A control parameter (Ψ) is generated which is equal to the sum of the square of the differences of the current temperature distribution of the test case (T') and the prior data set (i.e., temperature distribution (T) is utilized as the training data set). This Ψ term is a numerical value representing the magnitude of distance (in multiple dimensions) a given temperature distribution in a test set is from a temperature distribution in the training set (which is also termed as a “Radial Basis Function”/ “RBF” in multi-dimensions). For example, a larger Ψ term equates to a larger difference between the testing and training temperature distribution and a smaller Ψ term corresponds to a smaller difference between the respective test and training temperature distributions. Hence, during a melting duty cycle, for a given instant in time, the real-time temperature distribution values recorded by the thermocouple arrays are used in the algorithm as the test case to calculate the Ψ terms across the entire array of temperature distributions in the historical training dataset. With this, an array of Ψ terms is generated for all values in time of the temperature distributions from the training set. From this training data set, the temperature distribution with the lowest Ψ term has the closest affinity to the test case. Thus, the melt fraction value assigned to the temperature distribution from the training set which has the smallest Ψ term at that instant is assigned as the predicted melt fraction to the respective test set as it is the training data value which most closely matches the current test set (due to the minimization of the Ψ term). An example plot accruing from this technique is shown below. Fig. 8 shows a plot of the transient temperature profiles recorded by the three thermocouples within the testing apparatus during a melt cycle. The red arrow in the plot signifies a desired testing case to predict the melt fraction of the PCM at that instant (based on the temperature

history leading up to that instant in the experiment).

Based on this input temperature distribution as the test case, the machine learning algorithm was used to compare the compare the test case with the training data set (i.e., the entire set of temperature transients in temperature history contained in the training data set). This can be represented in an abstract sense, by generating Ψ terms encompassing all of the temperature transients in the training set. A visual example of this is provided in Fig. 9. The transient melt fraction from the training data set is plotted here. For each of these values of melt fraction at any instant, the respective values of the temperature transient are also associated from the training data in the RBF. Therefore, the Ψ terms generated during the experiments (the instantaneous temperature distribution at any instant within the recorded data is denoted by the red arrow in Fig. 6) are compared with that of the training data set (i.e., the temperature transients at a particular instant in time is plotted for the entire training data set). From this, the minimum value of the Ψ term can be obtained - which signifies that the particular training data for temperature distribution at this point most closely matches the testing temperature distribution (obtained in the experiment). Therefore, the respective melt fraction (used as the training label, which corresponds to the training temperature distribution data in the training dataset) with the lowest Ψ term is assigned as the predicted melt fraction (predicted value) for the chosen experimental data for temperature distribution (testing dataset). In Fig. 7, it can be seen that the Ψ term is lowest at the 66% melt fraction mark and respectively assigned as the predicted melt fraction. The actual melt fraction (as measured in the experiments) for that testing data set was 63%, thus demonstrating that the ML algorithm provided an accuracy of 95.2% for this particular instance. Additional examples are provided in the appendix for showing the plots of the temperature transients in the test data (used for making predictions for the instantaneous values of melt fraction). A selected temperature distribution at a particular instant in time and the generation of Ψ terms across all of the recorded times from the historical training dataset was used to establish the magnitude of correlation of the particular testing case to the melt fraction of the training data arrays. This method for predictions was performed for the entire array of testing temperature distribution data as well as for multiple testing data sets in order to develop statistics and quantitative metrics analyzing the accuracy and validity of the predictions shown in detail in the following sections. Furthermore, this method shows the feasibility of accurately predicting the melt fraction in real-time (with accuracies in excess of 95%) by utilizing the real-time temperature transient data within a TES for any duty cycle and during the melting of any PCM.

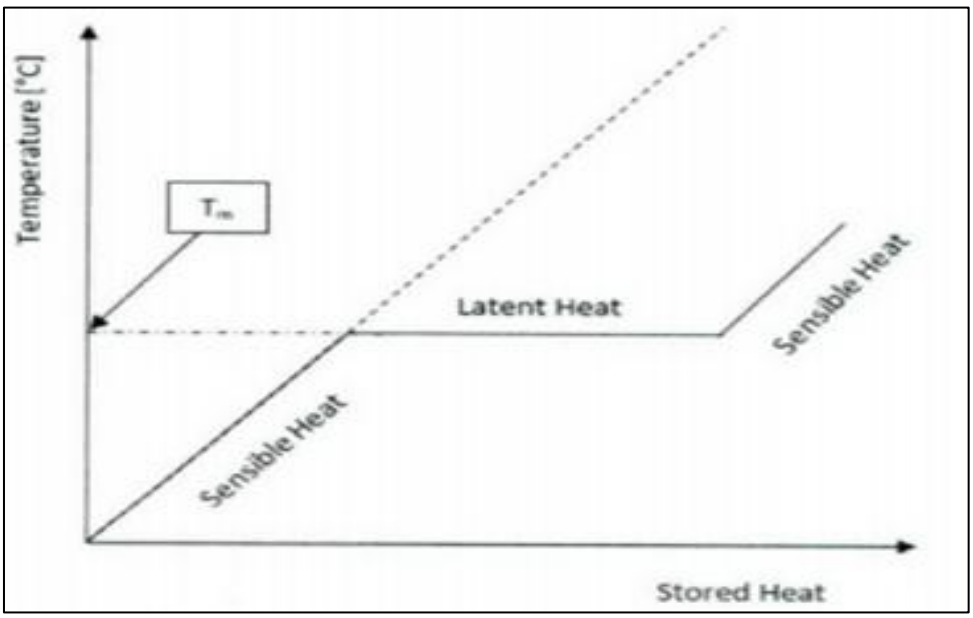

Fig. 1. Typical transient temperature profile (transient plot) for a PCM during the melting process [24]

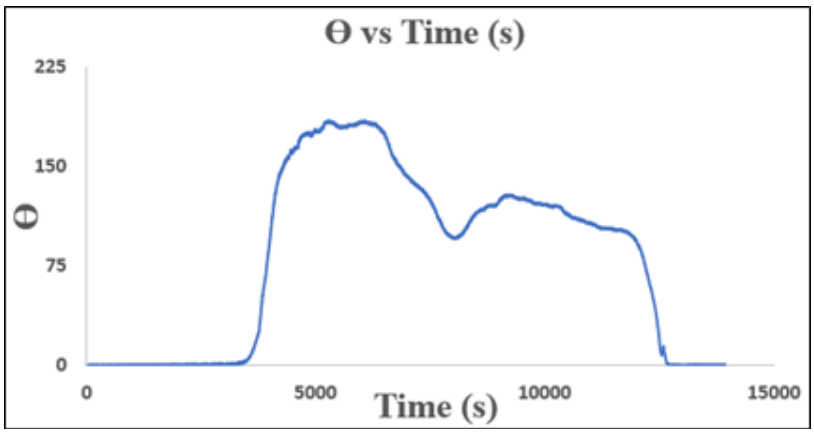

Fig. 2. Transient plot of θ (i.e., $[\Delta T]^2$)

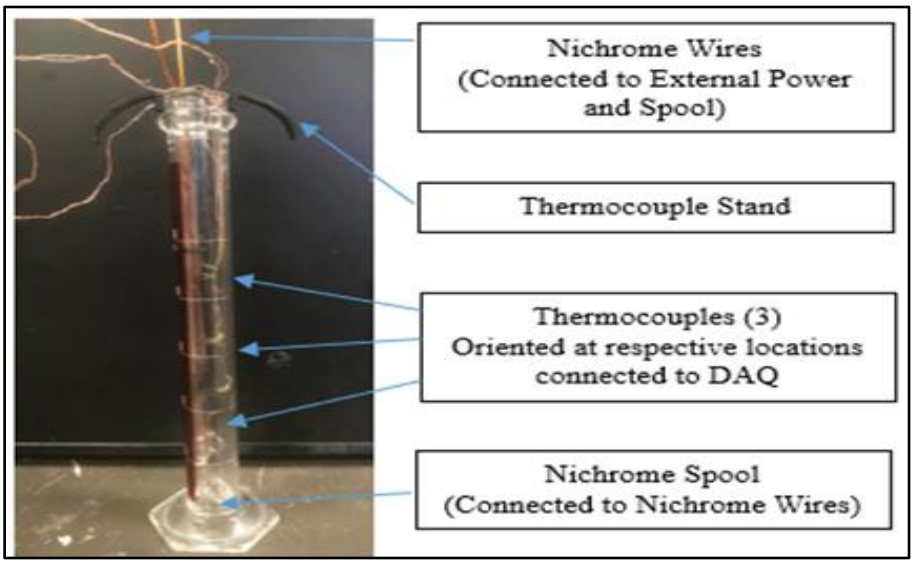

Fig. 3. Image of experimental apparatus used in this study

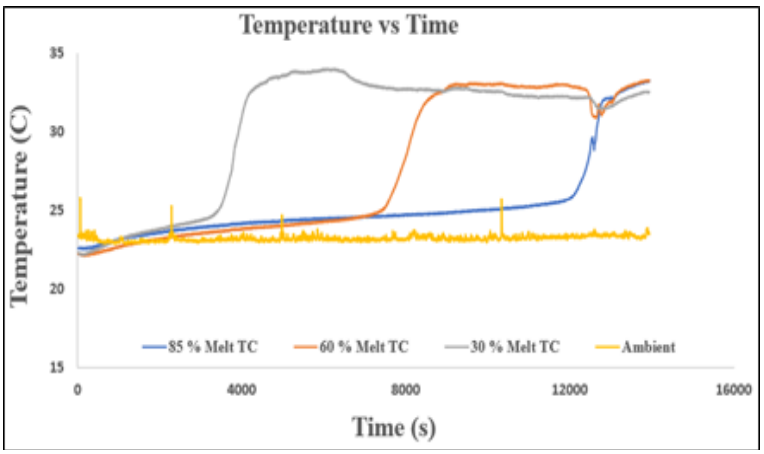

Fig. 4. A representative plot of temperature transients (in °C) recorded by the three thermocouples mounted at different vertical heights (corresponding to melt fractions of 30% [T_0], 60% [T_1] and 85% [T_2]) within the volume of the PCM contained in a measuring cylinder in the experimental apparatus

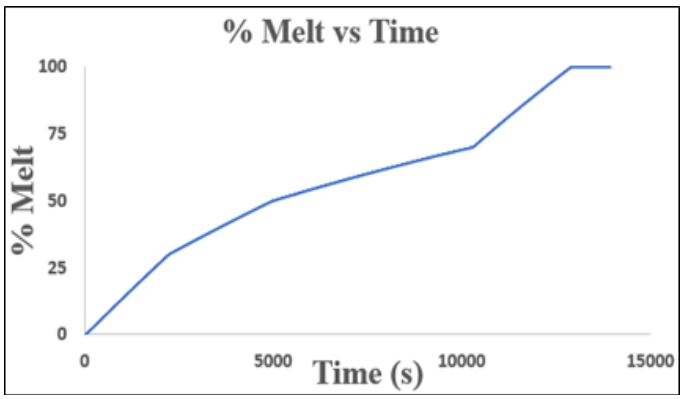

Fig. 5. Transient plot of melt fraction of PCM obtained from monitoring the height of liquid meniscus in the measuring cylinder using a digital camera

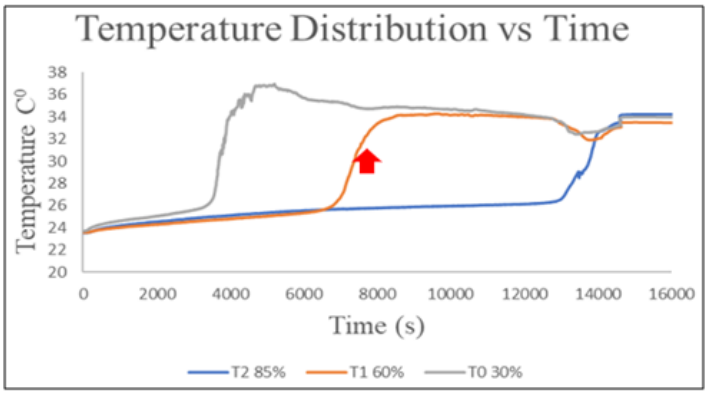

Fig. 6. Plot of experimental data (Testing Data) showing temperature transients recorded by three thermocouples located at heights corresponding to 30%, 60% and 85% melt fraction. Red arrow denotes chosen value of a specific test-data set that was utilized for melt fraction predictions, as shown in Fig. 7

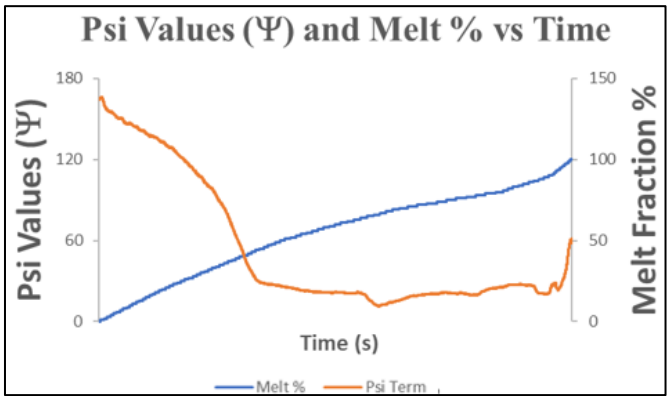

Fig. 7. Transient profile of *Ψ* and melt fraction (%) for the training dataset shown in Fig. 6. Melt fraction (%) is correlated with temperature distribution data (training data set). The plot shows that the values of the *Ψ* terms are calculated for the entire training dataset. Since the *Ψ* term represents the numerical magnitude for the difference in the temperature distributions of the training data set and a chosen testing data point, the minimum point in the global distribution for the *Ψ* profile (as shown in this plot) is identified and the respective melt fraction (%) from training data set correlating to this global minimum is assigned as the predicted melt fraction (%)

This method was cross tested for multiple duty cycles and demonstrated very promising results. After the propagating melt front reaches the location of the first thermocouple in the system (corresponding to 30% melt fraction), the prediction accuracies are above 85%. This accuracy increases as the melt front reaches the second and third thermocouples in the system. For example, the accuracy approaches 95% for the predictions from the machine learning (ML) model for values of melt fraction in the range of 85-100%. The melt fraction predictions before the melt front reaches the first thermocouple is lower, as there is no significant variation in the temperature data recorded by the array of three thermocouples. The prediction accuracies were improved with the incorporation of the θ parameter (i.e., values of θ $[\Delta T]^2$). Hence, it can be expected that the accuracy can be refined with the addition of more thermocouples in the array within the system (or by optimizing the location of the three thermocouples in the array).

The predictions from the ML algorithm were compared for cases incorporating the θ term (called ***Ψ***) with that of the cases not incorporating the θ term (called ***Ψ'***), as shown in Equations 2 and 3:

$$\psi = (T_0 - T_0')^2 + (T_1 - T_1')^2 + (T_2 - T_2')^2 + (\theta - \theta')^2 \quad (2)$$

$$\psi' = (T_0 - T_0')^2 + (T_1 - T_1')^2 + (T_2 - T_2')^2 \quad (3)$$

The figs. below show the predicted values of the melt fraction and are compared with the actual melt fractions from experimental data. Figs. 8 and 9 show the predictions and accuracies of the predicted values without the utilization of the θ parameter (called ***Ψ'***); while Figs. 10 and 11 are based on predictions incorporating the θ parameter (called ***Ψ***). Fig. 12 shows that the difference in the percent accuracy of the prediction with and without the θ parameter (i.e., Ψ versus Ψ'). Furthermore, the difference in accuracies between the two methods was estimated using equation 4 listed below.

$$\text{Accuracy (\%)} = \frac{Predicted\ Melt\ Fraction\ (\%)}{Actual\ Melt\ Fraction\ (\%)} \times 100 \quad (4)$$

An overall observable trend in the results is that the predicted accuracy is initially low; however, as the melt front reaches 30% (the location of the first thermocouple) there is a significant increase in the prediction accuracy (which is in excess of 85%). These further increases to values in excess of 90% as the melt front propagates and reaches locations of the additional thermocouples (even surpasses 95% as the system approaches complete melting). The graphs also show the increase in the percentage accuracy of the predictions when using the θ parameter (called Ψ), as opposed to not using the θ parameter (called Ψ'), especially for the initial stages of the melt cycle. It can be observed that there is a significant increase in accuracy as the melt front fraction progresses from the range of 0%-10% to the range of 30%-100%. However, for the melt fraction values in the range of 60%-100% there is only marginal improvement in the accuracy of the prediction.

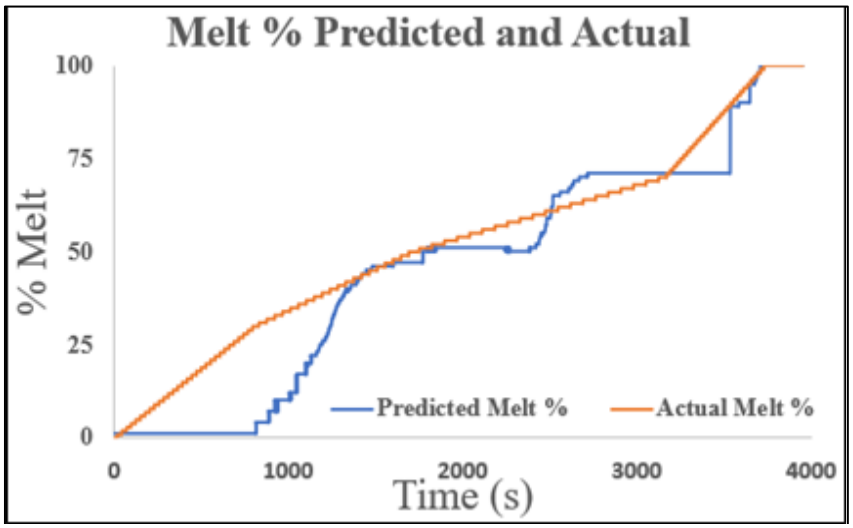

Fig. 8. Comparison of predicted values of melt fraction as a function of time to that of the actual values of melt fraction (obtained from experimental measurements) in machine learning (ML) model without using the θ parameter (called *Ψ'*)

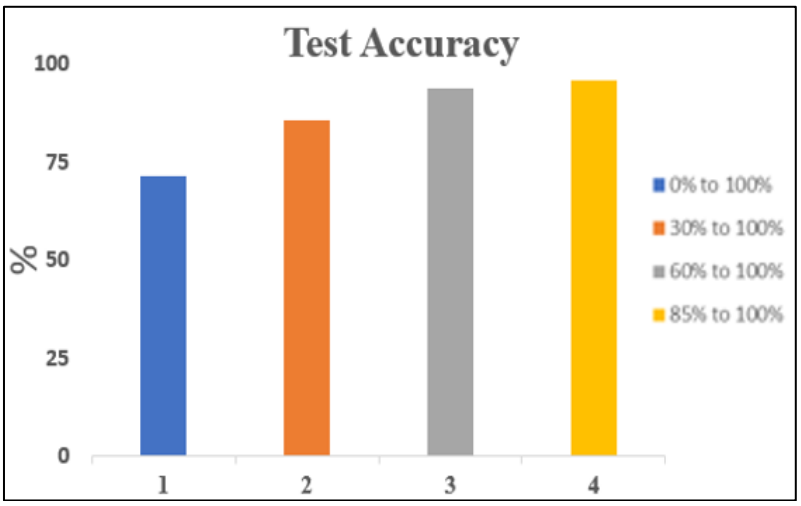

Fig. 9. Comparison of overall prediction accuracy (for the ML model without θ parameter, called *Ψ'*) for the different range of melt fractions

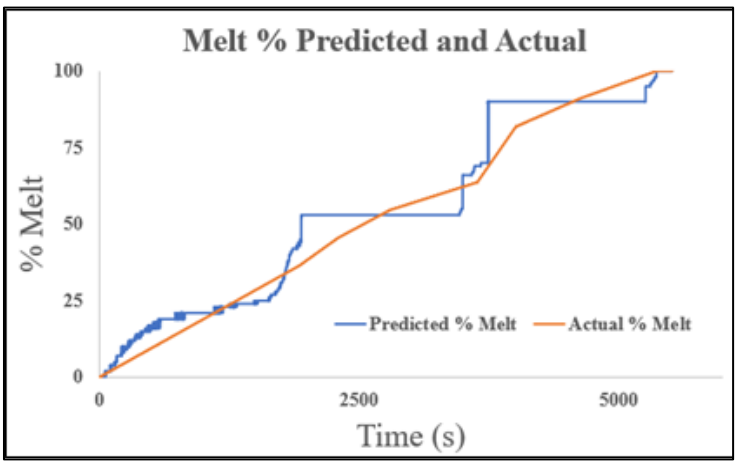

Fig. 10. Comparison of predicted values of melt fraction as a function of time to that of the actual values of melt fraction (obtained from experimental measurements) in machine learning (ML) model incorporating the θ parameter (called *Ψ*)

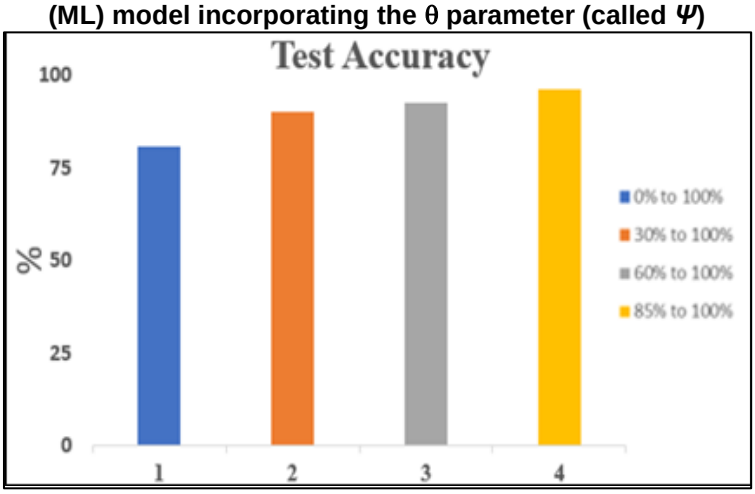

Fig. 11. Comparison of overall prediction accuracy (for the ML model with θ parameter, called *Ψ*) for the different range of melt fractions

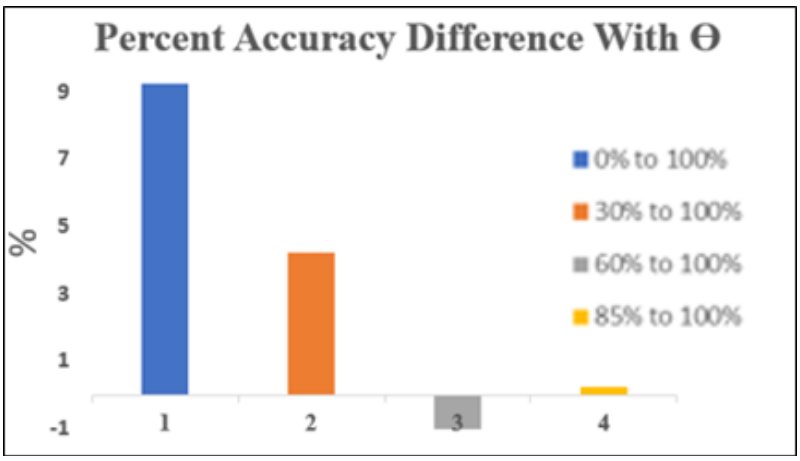

Fig. 12. Plot showing improvement in accuracy of predictions on incorporation of the θ parameter in the ML algorithm (Ψ versus Ψ'). substantial improvement in accuracy (~9%) is achieved for melt fractions in the range of 0-30% by incorporation of the θ parameter. However, no benefits are derived for higher melt fractions and yet higher computational costs are incurred by incorporation of the θ parameter

4. CONCLUSION

This study demonstrates the feasibility of using Machine Learning (ML) model based on RBF techniques [26] - for achieving high prediction accuracy for predicting the melt fraction of a specified mass of PCM based solely on the instantaneous measurement of transient temperature profile within a representative TES platform. This ML technique is based on the *supervised learning* approaches using an analogue to Radial Basis Functions (RBF) where a *nearest-neighbor approach* is utilized (i.e., using *similarity learning* that is based on *regression analysis*). The accuracy of this method is greater than 85% for determining the melt fraction of a PCM for the values of melt fractions in the range of 30-100%. Additionally, this accuracy increases as the melt fraction approaches 100%, which is attributed to the melt front reaching and passing additional thermocouples as it progresses through the PCM containment apparatus. The results of this study prove that ML techniques may be employed to be able to predict the melt fraction of a PCM within a TES unit which can be used as a tool to facilitate the implementation of inorganic PCMs to utilize their high latent heat capacity while mitigating the significant reliability issues concerning inorganic PCMs such as subcooling. Furthermore, the benefits of this method rely on its simplicity as there is no need for additional equipment (or additives to be added to the PCM). Competing techniques that rely on additional equipment (or require additives in the form of nucleators or gelling agents) will complicate the deployment/ operation while also increasing costs and compromise the effectiveness of such schemes due to the introduction of impurities within the PCM from these additives. Additional studies are currently being performed to further improve the prediction accuracy and incorporate additional parameters for improving the sophistication of the algorithm and enhancing the accuracy of the predictions (such as by comparing with negative-feedback control algorithms and proportional-integral-derivative/ PID control algorithms) for minimizing the fraction of un-melted PCM (i.e., without completely melting the PCM). This will help with determining the efficacy of this invention for maximizing the thermal energy storage capacity of a TES (using PCM) and also ensuring operational reliability while eliminating the need for subcooling of PCM. Moreover, the methodologies used in this study can have applications outside of TES in situations where there is a need for accurate real time complex system predictions based on previous historical systematic trends. The deployment of the Ψ term in the numerical scheme that was developed in this study - highlights the incorporation of a quantitative metric to compare the numerical similarity of particular multivariable parameters in multidimensional data, i.e., using an analogue of the Radial Basis Functions (RBF). Furthermore, the utilization of the weighting parameters can also improve the adaptability and robustness of this method based on specific complex system characteristics (which is a topic of future studies,

currently in progress in our research group). Therefore, the developed technique proves the feasibility of utilizing RBF based approaches, and demonstrates that RBF based real-time control schemes can provide accurate predictions in complex systems which typically exhibit nonlinear and chaotic characteristics in technological, social and biological phenomena to name a few.

ACKNOWLEDGEMENTS

This work was supported by the Multi-Phase Flow and Heat Transfer Laboratory (MPGHTL) under the supervision of Dr. Debjyoti Banerjee at Texas A&M University, College Station. Ms. M. Truong was supported by Research Experience for Undergraduates (REU) grant from the U.S. National Science Foundation (NSF).

COMPETING INTERESTS

Authors have declared that no competing interests exist.

REFERENCES

1. Adesina A. Use of phase change materials in concrete: current challenges, Renew. Energy Environ. Sustain. 2019;4(9)
2. Phase change materials and products for building applications: A state-of-the-art review and future research opportunities. Simen EdsjøKalnæsaBjørn Petter Jelleab; 2015.
3. Applications of phase change materials for sustainable energy | sustainability: A comprehensive foundation. Sustainability: A comprehensive foundation.
   Accessed: Jan.25, 2020
4. Ali S. Phase Change Materials: Limitations and Improvements; 2016.
5. Ryu HW, Woo SW, Shin BC. Kim SD, Sol. Energy Mater. Sol. Cells, 1992;27:161—172.
6. Xu X, Cui H, Memon SA, Yang H, Tang W, Energy Build., 2017;156:163—172.
7. Mohamed SA, Al-Sulaiman FA, Ibrahim NI, Zahir MH, Al-Ahmed A, Saidur R, Yılbaş BS, Sahin AZ, Renewable Sustainable Energy Rev. 2017;70:1072—1089.
8. Safari A, Saidur R, Sulaiman FA, Xu Y, Dong J. Renewable Sustainable Energy Rev. 2017;70:905—919.
9. Hussein A, Abd-Elhady MS, El-Sheikh MN et al. Improving heat transfer through paraffin wax, by using fins and metallic strips. Arab J Sci Eng 2018;43:4433–4441 Available:https://doi.org/10.1007/s13369-017-2923-2.
10. Tong Xinglin, Khan Jamil A, RuhulAmin M. Enhancement of heat transfer by inserting a metal matrix into a phase change material, Numerical Heat Transfer, Part A: Applications, 1996; 30(2):125-141,
    DOI: 10.1080/10407789608913832.
11. Yinping Z, Yi J, A simple method, the-history method, of determining the heat of fusion, specific heat and thermal conductivity of phase-change materials, Measurement Science and Technology, 1999;10(3):201.
12. Faucheux M, Muller G, Havet M, LeBail A. Influence of surface roughness on the supercooling degree: Case of selected water/ethanol solutions frozen on aluminium surfaces, International journal of refrigeration. 2006;29(7):1218-1224.
13. Taylor RA, Tsafnat N, Washer A. Experimental characterisation of sub-cooling in hydrated salt phase change materials, Applied Thermal Engineering. 2016;93:935-938.
14. García-Romero A, Diarce G, Ibarretxe J, Urresti A, Sala J. Influence of the experimental conditions on the subcooling of Glauber's salt when used as PCM, Solar energy materials and solar cells. 2012; 102:189-195.
15. Mehling H, Cabeza LF, Heat and cold storage with PCM. Springer; 2008.
16. Lane GA. Solar heat storage: Latent heat materials; 1983.
17. Shamberger PJ, Malley MJO. Heterogeneous nucleation of thermal storage material LiNO3· 3H2O from stable lattice-matched nucleation catalysts, Acta Materialia. 2015;84:265-274.
18. Shin BC, Kim SD, Won-Hoon P, Phase separation and supercooling of a latent heat-storage material, Energy. 1989;14 (12):921-930.
19. Schroder J, Gawron K. Heat storage material comprising calcium chloride-hexahydrate and a nucleating agent, ed: Google Patents; 1980.
20. Kimura H, Kai J, Phase change stability of CaCl2· 6H2O, Solar Energy. 1984;33 (1):49-55.
21. Lane, Phase change materials for energy storage nucleation to prevent supercooling, Solar energy materials and solar cells. 1992;27(2):135-160.

22. Meseguer J, Pérez-Grande I, Sanz-Andrés A. Spacecraft thermal control. Elsevier; 2012.
23. Günther E, Mehling H, Werner M, Melting and nucleation temperatures of three salt hydrate phase change materials under static pressures up to 800 MPa, Journal of Physics D: Applied Physics. 2007; 40(15):4636.
24. Kumar N, Banerjee D. A comprehensive review on salt hydrates as phase change materials (PCMs) ; 2018
25. Shettigar N†, Banerjee D, Truong M†, Thyagrajan A, Bamido A, Meza A et al. Application of machine learning for enhancing the transient performance of thermal energy storage platforms for obviating issues relating to the food-energy-water (few) nexus, Paper No. SHTC2020-9167, Proceedings of the ASME 2019 Summer Heat Transfer Conference (SHTC 2020), co-located with the Fluids Engineering Division Summer Meeting (FEDSM 2020), co-located with the International Conference on Nanochannels, Microchannels, and Minichannels (ICNMM 2020), July 12-15, 2020, Rosen Shingle Creek, Orlando, FL, USA; 2020.
26. Broomhead David H, Lowe David. Multivariable functional interpolation and adaptive networks (PDF). Complex Systems. Archived from the original (PDF) on 2014-07-14; 1988;2:321–355.

APPENDIX

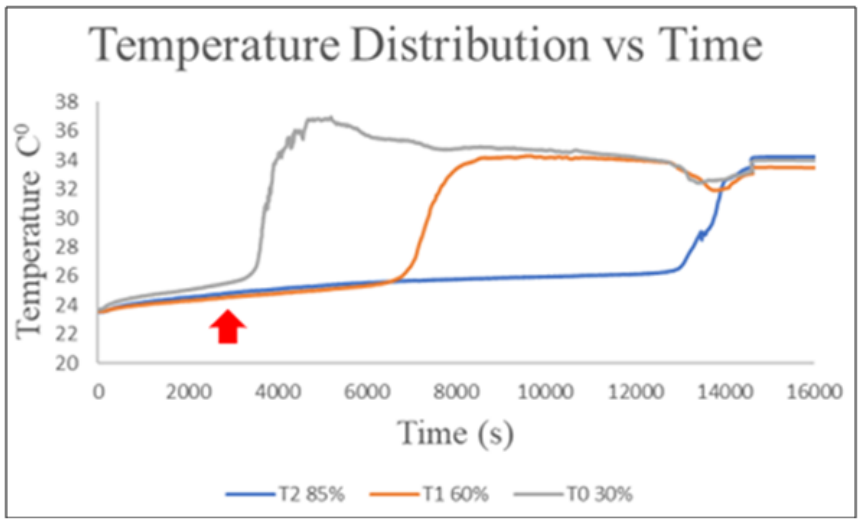

Fig. A1. Transient temperature distribution recorded in the melting experiments (testing dataset). Red arrow signifies selected temperature distribution for melt fraction prediction

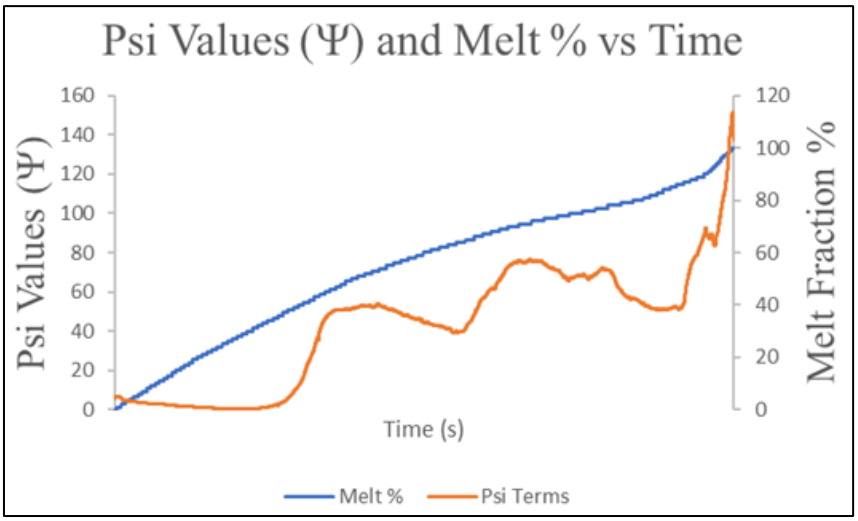

Fig. A2. Transient profile of Ψ term and melt fraction time corresponding to Fig. A1. Transient profile of melt fraction is from training dataset by correlating the temperature distribution from training dataset. Transient profile of Ψ term were generated for the specified time and corresponding temperature distribution (as a quantitative metric for identifying how similar the selected real-time temperature distribution is to historical training data sets). The melt fraction associated with the global minimum of the Ψ terms is assigned as the predicted melt fraction

Peer-review history:
The peer review history for this paper can be accessed here:
http://www.sdiarticle4.com/review-history/65675